

On the use of the local prior on the absolute magnitude of Type Ia supernovae in cosmological inference

David Camarena¹ and Valerio Marra^{2,3,4}

¹PPG_{Cosmo}, Universidade Federal do Espírito Santo, 29075-910, Vitória, ES, Brazil

²Núcleo de Astrofísica e Cosmologia & Departamento de Física, Universidade Federal do Espírito Santo, 29075-910, Vitória, ES, Brazil

³INAF – Osservatorio Astronomico di Trieste, via Tiepolo 11, 34131, Trieste, Italy

⁴IFPU – Institute for Fundamental Physics of the Universe, via Beirut 2, 34151, Trieste, Italy

Accepted XXX. Received YYY; in original form ZZZ

ABSTRACT

A dark-energy which behaves as the cosmological constant until a sudden phantom transition at very-low redshift ($z < 0.1$) seems to solve the $>4\sigma$ disagreement between the local and high-redshift determinations of the Hubble constant, while maintaining the phenomenological success of the Λ CDM model with respect to the other observables. Here, we show that such a hockey-stick dark energy cannot solve the H_0 crisis. The basic reason is that the supernova absolute magnitude M_B that is used to derive the local H_0 constraint is not compatible with the M_B that is necessary to fit supernova, BAO and CMB data, and this disagreement is not solved by a sudden phantom transition at very-low redshift. We make use of this example to show why it is preferable to adopt in the statistical analyses the prior on M_B as an alternative to the prior on H_0 . The three reasons are: i) one avoids potential double counting of low-redshift supernovae, ii) one avoids assuming the validity of cosmography, in particular fixing the deceleration parameter to the standard model value $q_0 = -0.55$, iii) one includes in the analysis the fact that M_B is constrained by local calibration, an information which would otherwise be neglected in the analysis, biasing both model selection and parameter constraints. We provide the priors on M_B relative to the recent Pantheon and DES-SN3YR supernova catalogs. We also provide a Gaussian joint prior on H_0 and q_0 that generalizes the prior on H_0 by SH0ES.

Key words: cosmological parameters–dark energy–cosmology: observations

1 INTRODUCTION

The Hubble constant H_0 – the first cosmographic coefficient in a series expansion of the scale factor – is perhaps the most basic parameter in cosmology. It is then understandable that the $>4\sigma$ disagreement between the local (Riess et al. 2021) and high-redshift (Aghanim et al. 2020) determinations of the Hubble constant has received much spotlight. Indeed, this tension could very well signal the need of a new standard model of cosmology, although it is not clear which alternative model can successfully explain all available observations (see Knox & Millea 2020; Di Valentino et al. 2021, for details).

A dark-energy which behaves as the cosmological constant until a sudden phantom transition at very-low redshift seems able to solve the H_0 crisis, while maintaining the phenomenological success of the Λ cold dark matter (CDM) model with respect to the other observables. The phenomenology of a late-time transition in the Hubble rate has been first considered by Mortonson et al. (2009), and recently confronted with data by Benevento et al. (2020);

Dhawan et al. (2020); Efstathiou (2021), while a low-redshift transition on the dark energy equation of state has been proposed by Alestas et al. (2020) (see also Keeley et al. 2019).

Here, we show that a hockey-stick¹ dark energy (h_s CDM, see Figure 1) cannot solve the H_0 crisis. The basic reason is that the supernova absolute magnitude M_B that is used to derive the local H_0 constraint is not compatible with the M_B that is necessary to fit supernova, baryon acoustic oscillations (BAO) and cosmic microwave background (CMB) data, and this remains true even with a sudden phantom transition at very-low redshift. Statistically, this becomes evident if one includes the supernova calibration prior on M_B in the statistical analysis, which would otherwise support h_s CDM.

We make use of this example to show in details why it is preferable to adopt the prior on M_B rather than the prior on H_0 in the cosmological analyses that study the impact of

¹ We remind the reader that a hockey stick trend is characterized by a sharp change after a relatively flat and quiet period.

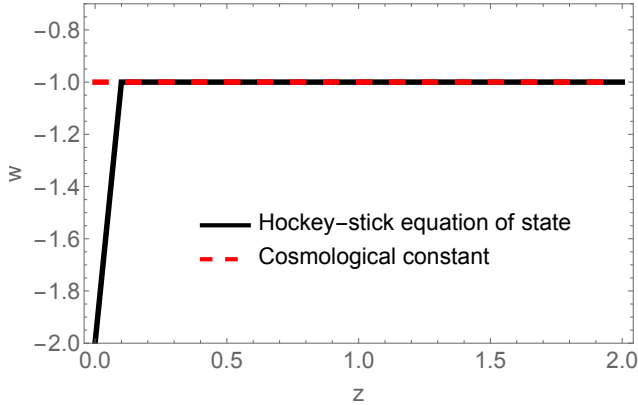


Figure 1. Hockey-stick dark energy behaves as the cosmological constant until a sudden phantom transition at very-low redshift.

local H_0 on the dark energy properties (see, for instance, the analysis performed in Section 5 of [Riess et al. 2016](#)). We also provide the M_B priors relative to the Pantheon and Dark Energy Survey Supernova Program (DES-SN3YR) catalogs, and a joint prior on H_0 and q_0 that generalizes the one on H_0 by the Supernova H0 for the Equation of State (SH0ES) collaboration.

This paper is organized as follows. In Section 2 we introduce hockey-stick dark energy, in Section 3 we discuss the prior on M_B , while in Section 4 we present the statistical analysis. The results are shown in Section 5 and the conclusions drawn in Section 6.

2 HOCKEY-STICK DARK ENERGY

In order to show the advantages of using a local prior on M_B instead of a local prior on H_0 we will consider a model that features a dark energy with the following hockey-stick equation of state ($hs\Lambda$ CDM):

$$w = \begin{cases} w_x - (1 + w_x)z/z_t & \text{if } z \leq z_t \text{ (the blade)} \\ -1 & \text{if } z > z_t \text{ (the shaft)} \end{cases}, \quad (1)$$

which mimics the cosmological constant at higher redshifts and deviates from the latter for $z \leq z_t$, reaching w_x at $z = 0$, see Figure 1. A step equation of state (constant w_x for $z \leq z_t$) shows a very similar phenomenology. Here, we adopt the hockey-stick equation of state as it features the same number of parameters (w_x and z_t) but is continuous. Models that feature the hockey-stick phenomenology are discussed in [Mortonson et al. \(2009\)](#).

It follows that the expansion rate is, assuming spatial flatness:

$$\frac{H^2(z)}{H_0^2} = \Omega_{M0}(1+z)^3 + \Omega_{R0}(1+z)^4 + \Omega_{\Lambda0}(1+z)^{3g(z)}, \quad (2)$$

where $\Omega_{M0} + \Omega_{R0} + \Omega_{\Lambda0} = 1$ and

$$g(z) = \frac{1}{\ln(1+z)} \int_0^z \frac{1+w(z')}{1+z'} dz' \quad (3)$$

$$= \frac{1+w_x}{z_t \ln(1+z)} \times \begin{cases} (1+z_t) \ln(1+z) - z & \text{if } z \leq z_t \\ (1+z_t) \ln(1+z_t) - z_t & \text{if } z > z_t \end{cases}.$$

The apparent magnitude is then:

$$m_B(z) = 5 \log_{10} \left[\frac{d_L(z)}{10 \text{pc}} \right] + M_B, \quad (4)$$

where the luminosity distance is:

$$d_L(z) = (1+z) \int_0^z \frac{c d\bar{z}}{H(\bar{z})}. \quad (5)$$

Finally, the distance modulus is given by:

$$\mu(z) = m_B(z) - M_B. \quad (6)$$

For $z_t \rightarrow \infty$ one recovers the w CDM model with $w = w_x$. We will consider the w CDM model for comparison sake.

3 SUPERNOVA CALIBRATION PRIOR

The determination of H_0 by the SH0ES Collaboration is a two-step process ([Riess et al. 2016](#)):

- (i) First, anchors, Cepheids and calibrators are combined to produce a constraint on the supernova Ia absolute magnitude M_B . This step only depends on the astrophysical properties of the sources.
- (ii) Second, Hubble-flow Type Ia supernovae in the redshift range $0.023 \leq z \leq 0.15$ are used to probe the luminosity distance-redshift relation in order to determine H_0 . Cosmography with $q_0 = -0.55$ and $j_0 = 1$ is adopted.

The latest constraint by SH0ES reads:

$$H_0^{\text{R21}} = 73.2 \pm 1.3 \text{ km s}^{-1} \text{Mpc}^{-1} \text{ (Riess et al. 2021)}. \quad (7)$$

Usually, one introduces in the cosmological analyses that use an H_0 prior the following χ^2 function:

$$\chi_{H_0}^2 = \frac{(H_0 - H_0^{\text{R21}})^2}{\sigma_{H_0^{\text{R21}}}^2}. \quad (8)$$

The goal of this paper is to show, using the example of hockey-stick dark energy, that it is preferable to skip step ii) above and adopt directly the local prior on M_B via:

$$\chi_{M_B}^2 = \frac{(M_B - M_B^{\text{R21}})^2}{\sigma_{M_B^{\text{R21}}}^2}, \quad (9)$$

where M_B^{R21} is the calibration that corresponds to the H_0 prior of equation (7).

Before proceeding, it is important to point out that supernovae Ia become standard candles only after standardization and that the method used to fit supernova Ia light curves, and its parameters, can influence the inferred value of M_B (e.g., x_0 , x_1 and c in the case of SALT2, [Guy et al. 2007](#)). This means that the actual prior on M_B from SH0ES can only be used with the Supercal supernova sample ([Scolnic et al. 2015](#)), which is the one adopted by SH0ES in the latest analyses.

Consequently, in order to meaningfully use the local prior on M_B , one has to translate it to the light curve calibration adopted by some other dataset X. This task can be achieved using the method developed in [Camarena & Marra \(2020a\)](#): the basic idea is to demarginalize the final H_0 measurement using for step ii) the supernovae of the dataset X that are in the same redshift range $0.023 \leq z \leq 0.15$.

SN dataset	Reference	Effective prior on M_B^{R21}
Supercal	Scolnic et al. (2015)	-19.2421 ± 0.0375 mag
Pantheon	Scolnic et al. (2018)	-19.2435 ± 0.0373 mag
DES-SN3YR	Brout et al. (2019)	-19.2389 ± 0.0336 mag

Table 1. Effective prior on M_B to be used instead of the prior on H_0 by Riess et al. (2021) when carrying out cosmological inference with the corresponding supernova dataset. Code and up-to-date values available at github.com/valerio-marra/CalPriorSNIa.

This procedure, applied to the latest supernova catalogs, produces the priors listed in Table 1. In other words, by adopting the priors given in Table 1 and performing step ii), one recovers the H_0 determination of equation (7).

It is worth mentioning that supernovae Ia are not perfectly standardizable candles and there are residual correlations with their environment, such as the step correction to M_B according to the host galaxy mass (Kelly et al. 2010; Lampeitl et al. 2010; Sullivan et al. 2010). The method discussed in this section assumes that these residual corrections have been applied before obtaining the effective prior on M_B .

Correlations between the residuals and the supernova environment have also been used to argue in favor of a possible time evolution of the absolute magnitude (Kang et al. 2020; Kim et al. 2019). Recent analyses suggest that such time evolution is not favored by data (Huang 2020; Koo et al. 2020; Sapone et al. 2020) and could have been produced by systematics (Brout & Scolnic 2021; Rose et al. 2020). Throughout this work we assume that M_B does not evolve with time.

3.1 Local joint H_0 - q_0 constraint

Although, as we argue below, it is preferable to use in the statistical analysis the prior on M_B , it is nevertheless important to determine the local value of H_0 .

The measurement by SHOES of equation (7) is obtained from the local constraint on M_B after adopting in the cosmographic analysis the following Dirac delta prior on the deceleration parameter q_0 :

$$f(q_0) = \delta(q_0 - q_{0,\text{fid}}), \quad (10)$$

$$q_{0,\text{fid}} = \frac{3}{2}\Omega_{M0,\text{fid}} - 1 = -0.55, \quad (11)$$

where the deceleration parameter takes the value relative to the flat concordance Λ CDM model with $\Omega_{M0,\text{fid}} = 0.3$ (Riess et al. 2016). In other words, the constraint of equation (7) uses information beyond the local universe in order to fix the value of q_0 .

One can improve the local determination of H_0 by adopting an uninformative prior $f(q_0) = \text{constant}$. Specifically, adopting the M_B prior relative to the Supercal dataset given in Table 1 and the same 217 Supercal supernovae used by SHOES, one obtains the joint prior that is given in Table 2 and illustrated in Figure 2. This constraint on H_0 and the CMB-only constraint from the Planck Collaboration (Aghanim et al. 2020) disagree at the 4.5σ level.

parameter	$\mu_i \pm \sigma_i$	C_{ij}	
H_0 [$\frac{\text{km/s}}{\text{Mpc}}$]	74.30 ± 1.45	1	-0.41
q_0	-0.91 ± 0.22	-0.41	1

Table 2. Joint prior on H_0 and q_0 , marginalized over the supernova absolute magnitude M_B . $\mu_i \pm \sigma_i$ are the marginalized mean values and standard deviation for the parameters, while C_{ij} is the correlation matrix. The covariance matrix is given by $\Sigma_{ij} = \sigma_i \sigma_j C_{ij}$ (without summation). This determination of H_0 generalizes the one of equation (7) by SHOES.

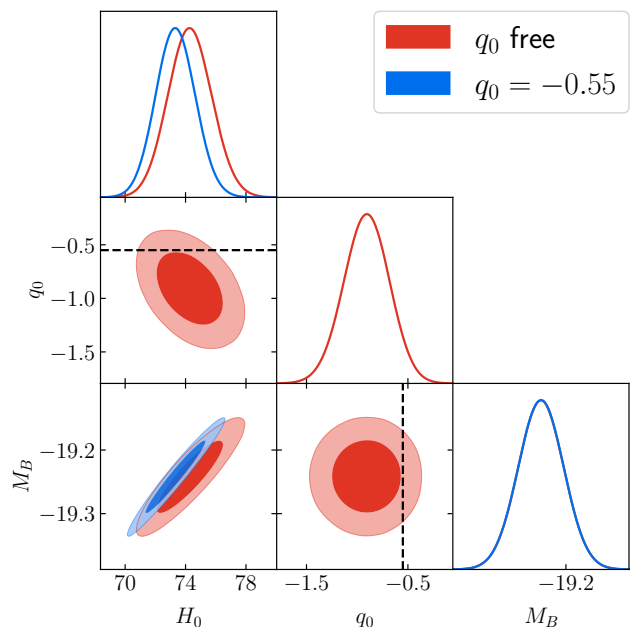


Figure 2. Marginalized local constraints on H_0 , q_0 and M_B (in red). If the deceleration parameter is fixed to $q_0 = -0.55$, one obtains the original H_0 constraint by SHOES (in blue).

We have used the numerical codes `emcee` (Foreman-Mackey et al. 2013) and `getdist` (Lewis 2019).

It is worth noting that the determination of Table 2 only assumes large-scale homogeneity and isotropy and no information from observations beyond the local universe is used. For comparison, we show in Figure 2 also the original constraint of equation (7) that is recovered by fixing $q_0 = -0.55$.² Note also that M_B shows basically no correlation with q_0 . In other words, fixing $q_0 = -0.55$ (Riess et al. 2021) should not have biased the determination of M_B via the method of Camarena & Marra (2020a).

² To be precise, the constraint of equation (7) adopts third-order cosmography and fixes also $j_0 = 1$. As in Figure 2 we use second-order cosmography, fixing $q_0 = -0.55$ gives back an H_0 that is $0.1 \text{ km s}^{-1} \text{ Mpc}^{-1}$ higher than the one of equation (7).

4 STATISTICAL INFERENCE

We now discuss the datasets that we adopt in order to constrain the hs CDM model.

4.1 Cosmic Microwave Background

We use the Gaussian prior on $(R, l_a, \Omega_{B0} h^2, n_s)$ derived from the Planck 2018 results (Chen et al. 2019, w CDM model in Table I). We denote with χ_{cmb}^2 the corresponding χ^2 function.

4.2 Baryonic Acoustic Oscillations

We adopt BAO measurements from the following surveys: 6dFGS (Beutler et al. 2011), SDSS-MGS (Ross et al. 2015) and BOSS-DR12 (Alam et al. 2017). 6dFGS and SDSS-MGS provide isotropic measurements at redshifts 0.1 and 0.15, while BOSS-DR12 data constrains $H(z)$ and $d_A(z)$ at redshifts 0.38, 0.51 and 0.61. We denote with χ_{bao}^2 the corresponding χ^2 function.

4.3 Supernovae Ia

We consider the Pantheon dataset, consisting of 1048 Type Ia supernovae spanning the redshift range $0.01 < z < 2.3$ (Scolnic et al. 2018). We denote with χ_{sne}^2 the corresponding χ^2 function.

4.4 Local constraint

We will consider either the prior on H_0 of equation (8) or the prior on M_B of equation (9) relative to the Pantheon sample, see Table 1.

4.5 Total likelihood: M_B vs H_0

The main goal of this paper is to show how the result of the analysis is biased when using $\chi_{H_0}^2$ instead of $\chi_{M_B}^2$. To this end we will build and compare the following two likelihoods:

$$\chi_{\text{tot}, H_0}^2(\theta) = \chi_{\text{cmb}}^2 + \chi_{\text{bao}}^2 + \chi_{\text{sne}}^2 + \chi_{H_0}^2, \quad (12)$$

$$\chi_{\text{tot}, M_B}^2(\theta) = \chi_{\text{cmb}}^2 + \chi_{\text{bao}}^2 + \chi_{\text{sne}}^2 + \chi_{M_B}^2. \quad (13)$$

Note that the number of data points is the same for both analyses.

In both cases the parameter vector is:

$$\theta = \{H_0, \Omega_{M0}, w_x, z_t, M_B, \Omega_{B0}, n_s\}. \quad (14)$$

In particular, the posteriors are not marginalized analytically over M_B so that we can obtain the posterior on M_B . However, it is often computationally useful to marginalize the posterior over M_B and in the next Section we present the corresponding formulas.

4.6 Posterior marginalized over M_B

In the case of the χ_{tot, H_0}^2 of equation (12), it is well known that one can marginalize analytically the posterior over M_B (Goliath et al. 2001). As we will show below, this is possible also for the χ_{tot, M_B}^2 of equation (13). For completeness we will present both cases.

4.6.1 Prior on H_0

Since, in this case, M_B enters only the SN likelihood, we will consider only the latter. The χ^2 function is:

$$\chi_{\text{sne}}^2 = \{m_{B,i} - m_B(z_i)\} \Sigma_{\text{sne},ij}^{-1} \{m_{B,j} - m_B(z_j)\} \\ = \{y_i - M_B\} \Sigma_{\text{sne},ij}^{-1} \{y_j - M_B\}, \quad (15)$$

$$y_i = m_{B,i} - \mu(z_i), \quad (16)$$

where the apparent magnitudes $m_{B,i}$, redshifts z_i and covariance matrix Σ_{sne} are from the Pantheon catalog (considering both statistical and systematic errors).

In the standard analysis one adopts an improper prior on M_B and integrate over the latter:

$$\mathcal{L}_{\text{sne}}^{\text{marg}} \propto \int_{-\infty}^{+\infty} dM_B \exp \left[-\frac{1}{2} \chi_{\text{sne}}^2 \right] \quad (17) \\ = \int_{-\infty}^{+\infty} dM_B \exp \left[-\frac{1}{2} (S_2 - 2M_B S_1 + M_B^2 S_0) \right] \\ \propto \exp \left[-\frac{1}{2} \left(S_2 - \frac{S_1^2}{S_0} \right) \right],$$

where inconsequential cosmology-independent factors have been neglected and we defined the auxiliary quantities:

$$S_0 = V_1 \cdot \Sigma_{\text{sne}}^{-1} \cdot V_1^T, \\ S_1 = y \cdot \Sigma_{\text{sne}}^{-1} \cdot V_1^T, \\ S_2 = y \cdot \Sigma_{\text{sne}}^{-1} \cdot y^T, \quad (18)$$

where V_1 is a vector of unitary elements. Equivalently, one can use the following new χ^2 function instead of χ_{sne}^2 :

$$\chi_{\text{sne, marg}}^2 = S_2 - \frac{S_1^2}{S_0}, \quad (19)$$

which does not depend on H_0 .

4.6.2 Prior on M_B

In the case of the χ_{tot, M_B}^2 of equation (13), M_B enters the supernova likelihood and the M_B likelihood, which have to be integrated over at the same time:

$$\mathcal{L}_{\text{sne+loc}}^{\text{marg}} \propto \int_{-\infty}^{+\infty} dM_B \exp \left[-\frac{1}{2} (\chi_{\text{sne}}^2 + \chi_{M_B}^2) \right] \quad (20) \\ = \exp \left[-\frac{1}{2} \left(S_2 - \frac{S_1^2}{S_0} \right) \right] \times \\ \int_{-\infty}^{+\infty} dM_B \exp \left[-\frac{1}{2} \frac{(M_B - \frac{S_1}{S_0})^2}{S_0^{-1}} - \frac{1}{2} \frac{(M_B - M_B^{\text{R21}})^2}{\sigma_{M_B}^2} \right] \\ = \exp \left[-\frac{1}{2} \left(S_2 - \frac{S_1^2}{S_0} + \frac{(S_1/S_0 - M_B^{\text{R21}})^2}{S_0^{-1} + \sigma_{M_B}^2} \right) \right],$$

where again inconsequential cosmology-independent factors have been neglected.

Equivalently, one can use the following new χ^2 function instead of $\chi_{\text{sne}}^2 + \chi_{M_B}^2$:

$$\chi_{\text{sne+loc, marg}}^2 = \chi_{\text{sne, marg}}^2 + \chi_{\text{loc}}^2, \quad (21)$$

where

$$\chi_{\text{loc}}^2 = \frac{(S_1/S_0 - M_B^{\text{R21}})^2}{S_0^{-1} + \sigma_{M_B}^2}. \quad (22)$$

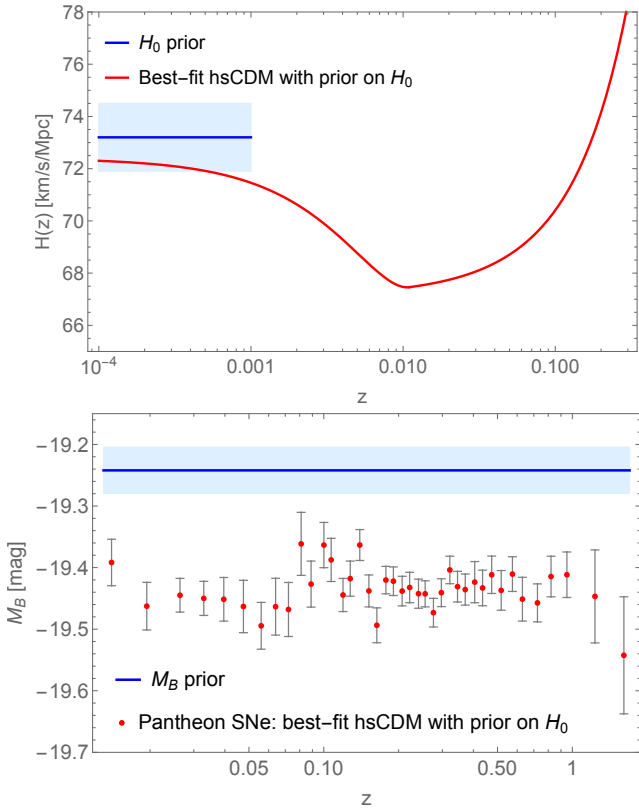


Figure 3. Hubble rate and the inferred absolute magnitudes $M_{B,i} = m_{B,i} - \mu(z_i)$ for the best-fit $hsCDM$ model when using the prior on H_0 (Table 3, top). For clarity we are showing the binned version of the Pantheon catalog (the statistical analysis uses the full sample). One can see that, even though the best-fit H_0 agrees well with the H_0 prior (top), the inferred $M_{B,i}$ do not agree with the local prior on M_B (bottom).

Note that χ_{loc}^2 does depend on H_0 . In particular, it is interesting to consider the case of a diagonal covariance matrix $\Sigma_{sne} = \sigma^2 \mathbf{1}$, where $\mathbf{1}$ is the $n \times n$ identity matrix. In this case one has:

$$\chi_{loc}^2 = \frac{\left[5 \log_{10} H_0 - M_B^{R21} + \frac{1}{n} \sum_i \left(m_{B,i} - 5 \log_{10} \frac{H_0 d_{L,i}}{10 \text{pc}} \right) \right]^2}{\sigma^2/n + \sigma_{M_B}^2} \quad (23)$$

The term within round brackets does not depend on H_0 but is a cosmology-dependent intercept that affects the determination of H_0 via the local calibration M_B^{R21} . Finally, the error is just the sum in quadrature of the calibration and intercept errors.

5 RESULTS

Table 3 shows a comparison between the best fits relative to the analyses of equations (12) and (13). Our results are obtained using the numerical codes CLASS (Blas et al. 2011), MontePython (Audren et al. 2013) and getdist (Lewis 2019).

When using the prior on H_0 (Table 3, top), the $hsCDM$ model, with an extremely phantom $w_x \simeq -14$, features a

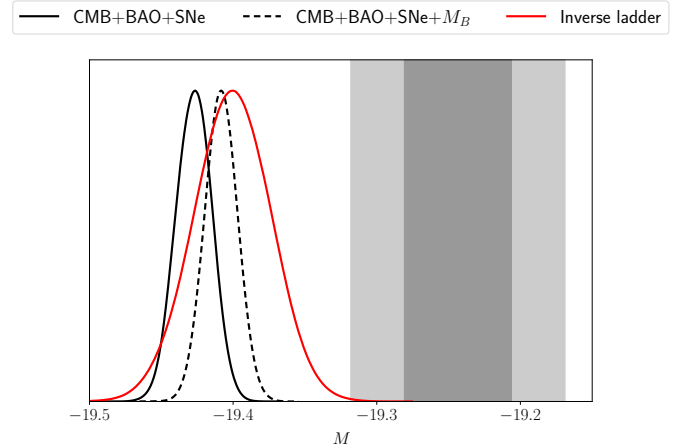


Figure 4. The posteriors on M_B from the analyses of the $hsCDM$ model (black line) and the inverse-distance ladder (red line) are in disagreement with the local prior from Table 1 (grey contour). This robustly shows that the SN calibration produced by CMB and BAO is in tension with the local astrophysical calibration. This remains true if a local prior on M_B is used in the analysis of the $hsCDM$ model (black dashed line): the difficulty in matching the local calibration is the source of the H_0 crisis.

significantly lower minimum χ^2 as compared to the $wCDM$ model. In particular, the disagreement with respect to the SH0ES determination of equation (7) is completely resolved. The phantom transition seems to have explained away the H_0 crisis. However, the best-fit M_B is 5σ away from the prior on M_B from Table (1), and this information is not included in the total χ^2 . This biases both model selection and the best-fit model. To better illustrate this point, we show in Figure 3 the Hubble rate and the inferred absolute magnitudes $M_{B,i} = m_{B,i} - \mu(z_i)$ for the best-fit $hsCDM$ model. Even though the best-fit H_0 agrees well with the H_0 prior (Figure 3, top), the inferred $M_{B,i}$ do not agree with the local prior on M_B throughout the full redshift range (Figure 3, bottom).

When, instead, the $\chi_{M_B}^2$ of equation (9) is adopted (Table 3, bottom), the $hsCDM$ model features the same best-fit H_0 of the $wCDM$ model, both 3σ away from the SH0ES determination of equation (7). Moreover, the $hsCDM$ has a worse overall fit to the data as compared to $wCDM$. In other words, hockey-stick dark energy neither solves the H_0 crisis nor manifests any statistical advantage with respect to $wCDM$.

From these results it is clear what is the source of the Hubble crisis. CMB and BAO constrain tightly the luminosity distance-redshift relation and so the distance modulus $\mu(z)$. The Pantheon dataset constrains the supernova apparent magnitudes m_B . Consequently, CMB, BAO and SNe produce a calibration on M_B which happens to be in strong disagreement with the local astrophysical calibration via Cepheids (see Figure 3 and Table 3). This disagreement was highlighted by Camarena & Marra (2020b, Figure 5) where the inverse-distance ladder technique was used to propagate the CMB constraint on r_d to M_B in a parametric-free way. Figure 4 shows how the constraint on M_B from the

Analysis with prior on H_0	$\hat{\chi}_{\text{cmb}}^2$	$\hat{\chi}_{\text{bao}}^2$	$\hat{\chi}_{\text{sne}}^2$	$\hat{\chi}_{H_0}^2$	$\hat{\chi}_{\text{tot}}^2$	$\Delta\hat{\chi}^2$	best-fit vector $\{H_0, \Omega_{M0}, w_x, z_t, M_B, \Omega_{B0}, n_s\}$	distance from H_0^{R21}	distance from M_B^{R21}
$w\text{CDM}$	2.9	5.1	1030.0	7.8	1045.8	0	{69.6, 0.29, -1.08, —, -19.39, 0.046, 0.97}	2.8	3.8
$hs\text{CDM}$	1.3	5.9	1027.7	0.3	1035.1	-10.7	{72.5, 0.26, -14.4, 0.010, -19.42, 0.043, 0.97}	0.5	4.9
Analysis with prior on M_B	$\hat{\chi}_{\text{cmb}}^2$	$\hat{\chi}_{\text{bao}}^2$	$\hat{\chi}_{\text{sne}}^2$	$\hat{\chi}_{M_B}^2$	$\hat{\chi}_{\text{tot}}^2$	$\Delta\hat{\chi}^2$	best-fit vector $\{H_0, \Omega_{M0}, w_x, z_t, M_B, \Omega_{B0}, n_s\}$	distance from H_0^{R21}	distance from M_B^{R21}
$w\text{CDM}$	2.8	5.2	1029.3	14.6	1051.9	0	{69.4, 0.29, -1.07, —, -19.39, 0.047, 0.97}	2.9	3.8
$hs\text{CDM}$	1.8	7.1	1027.1	19.4	1055.4	3.5	{69.3, 0.29, -1.73, 0.055, -19.41, 0.047, 0.97}	3.0	4.4

Table 3. Comparison between the best fits relative to the analyses of equations (12) (top) and (13) (bottom). A hat denotes the minimum χ^2 . The $\Delta\hat{\chi}^2$ values are computed with respect to $w\text{CDM}$. The last two columns give the σ -distance $(H_0^{\text{R21}} - H_0^{\text{bf}})/\sigma_{H_0^{\text{R21}}}$ and $(M_B^{\text{R21}} - M_B^{\text{bf}})/\sigma_{M_B^{\text{R21}}}$ from the values given in equation (7) and Table (1) (Pantheon), respectively.

inverse-distance ladder analysis agrees with the one relative to the $hs\text{CDM}$ model.

Finally, Figures 5 and 6 show how Bayesian inference changes when one adopts the prior on M_B instead of the prior on H_0 . The impact on the analysis relative to $w\text{CDM}$ is minimal, suggesting the validity of previous analyses of the $w\text{CDM}$ model that adopted the prior on H_0 . On the other hand, the constraints relative to the $hs\text{CDM}$ model change significantly. The impact on w_x is particular strong: in the case of the analysis with the prior on H_0 much more phantom values of w_x are allowed as compared with the analysis with the prior on M_B . Also note that the analysis with M_B includes $z_t = 0.1$ at 2σ level while the analysis with H_0 constrains $z_t < 0.06$ at 2σ level, showing a preference for a low-redshift transition. In other words, in the case of models with a low-redshift transition, the use of the prior on H_0 both biases model selection and distorts the posterior. In the analysis we adopted the flat prior $0.01 \leq z_t \leq 0.1$ (Benevento et al. 2020; Alestas et al. 2020): a transition at redshifts lower than 0.01 would not affect the determination of H_0 and a transition at redshifts higher than 0.1 would not solve the H_0 crisis, as also shown by Figure 6 (blue curve).

6 CONCLUSIONS

In this paper we clearly show that a sudden phantom transition at very-low redshift cannot solve the $>4\sigma$ disagreement between the local and high-redshift determinations of the Hubble constant. This point has been previously made by Benevento et al. (2020) in the contest of a sudden low-redshift discontinuity in the expansion rate, and by Lemos et al. (2019) who showed through an $H(z)$ reconstruction that SN, BAO and r_d constraints do not allow for a higher expansion rate at low redshifts (see also the recent analysis by Efstathiou 2021).³

Here, we single out the reason of this failure in solving the H_0 crisis: the supernova absolute magnitude M_B that is used to derive the local H_0 constraint is not compatible with the M_B that is necessary to fit supernova, BAO and

CMB data, see Figures 3 and 4. Statistically, this incompatibility is taken into account in the analysis if one adopts the supernova calibration prior on M_B instead of the prior on H_0 .

For completeness, we wish to summarize the three reasons why one should use the $\chi_{M_B}^2$ of equation (9) instead of the $\chi_{H_0}^2$ of equation (8):⁴

- (i) The use of $\chi_{M_B}^2$ avoids potential double counting low-redshift supernovae: for example, there are 175 supernovae in common between the Supercal and Pantheon datasets in the range $0.023 \leq z \leq 0.15$, and, in the standard analysis, these supernovae are used twice: once for the H_0 determination and once when constraining the cosmological parameters. This induces a covariance between H_0 and the other parameters which could bias cosmological inference.
- (ii) The supernova calibration prior on M_B is an astrophysical and local measurement. The determination of H_0 is instead based on a cosmographic analysis and it depends on a) its validity and b) its priors (SH0ES adopts $q_0 = -0.55$). While one can relax b) and obtain a joint H_0 - q_0 prior (see Table 2), the cosmographic analysis may fail for models with sudden transitions such as $hs\text{CDM}$. As $\chi_{M_B}^2$ is not based on a cosmographic analysis, it does not suffer from these issues.
- (iii) Most importantly, the use of $\chi_{M_B}^2$ guarantees that one includes in the analysis the fact that M_B is constrained by the calibration prior of Table (1).

While, as shown by Table 3 and Figures 5 and 6, the conclusions for $w\text{CDM}$ are not changed when $\chi_{M_B}^2$ is adopted, the use of $\chi_{M_B}^2$ becomes compelling when more exotic models are investigated; the use of $\chi_{H_0}^2$ can indeed lead to incorrect conclusions. Given that using $\chi_{M_B}^2$ does not add any statistical complexity to the analysis (see equation (21)), we encourage the community to adopt this prior in all the analyses. However, one should bear in mind that one must adopt the prior on M_B that corresponds to the supernova dataset that one wishes to adopt in their statistical analysis. These can be obtained using the code made available at github.com/valerio-marra/CalPriorSNIa, where we

³ Similar conclusions can be derived from the non-parameter inverse distance ladder analysis of Camarena & Marra (2020b), which shows that the calibration given by CMB and BAO to SN does not agree with the one by Cepheid distances, see Fig. 4.

⁴ Some of these points were previously raised by Camarena & Marra (2020a); Benevento et al. (2020).

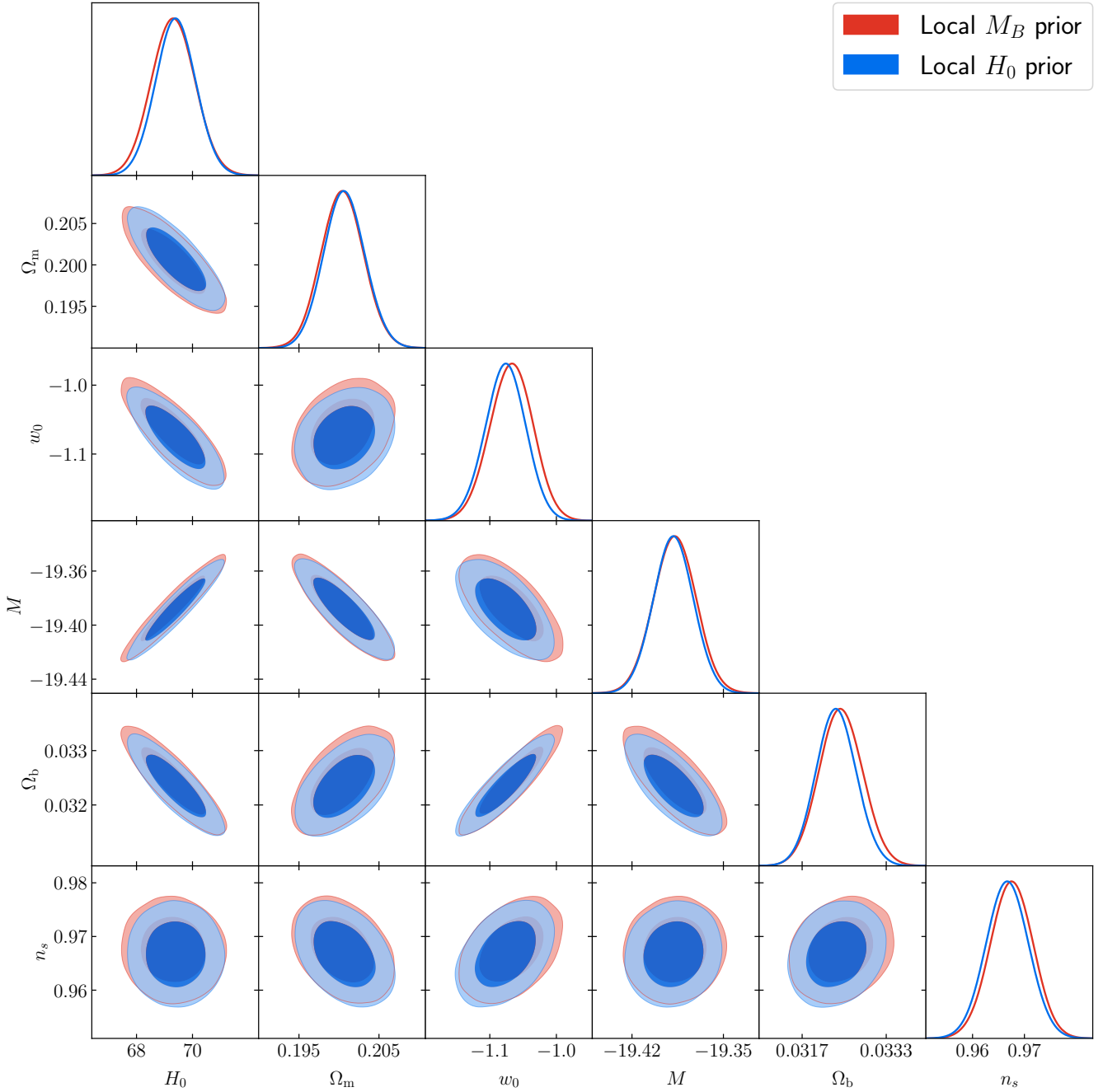


Figure 5. Marginalized constraints for the w CDM model from CMB, BAO, SNe and local observations. The two sets of contours show the analysis that adopts the prior on M_B of equation (9) and the one that adopts the prior on H_0 of equation (8).

will keep an updated list of the M_B priors that correspond to the latest supernova catalogs.

ACKNOWLEDGEMENTS

It is a pleasure to thank Leandros Perivolaropoulos, Adam Riess, Sunny Vagnozzi and Adrià Gómez-Valent for useful comments and discussions. DC thanks CAPES for financial support. VM thanks CNPq and FAPES for partial financial support. This project has received funding from the Eu-

ropean Union’s Horizon 2020 research and innovation programme under the Marie Skłodowska-Curie grant agreement No 888258. This work also made use of the Virgo Cluster at Cosmo-ufes/UFES, which is funded by FAPES and administrated by Renan Alves de Oliveira.

DATA AVAILABILITY

The data underlying this article will be shared on reasonable request to the corresponding author.

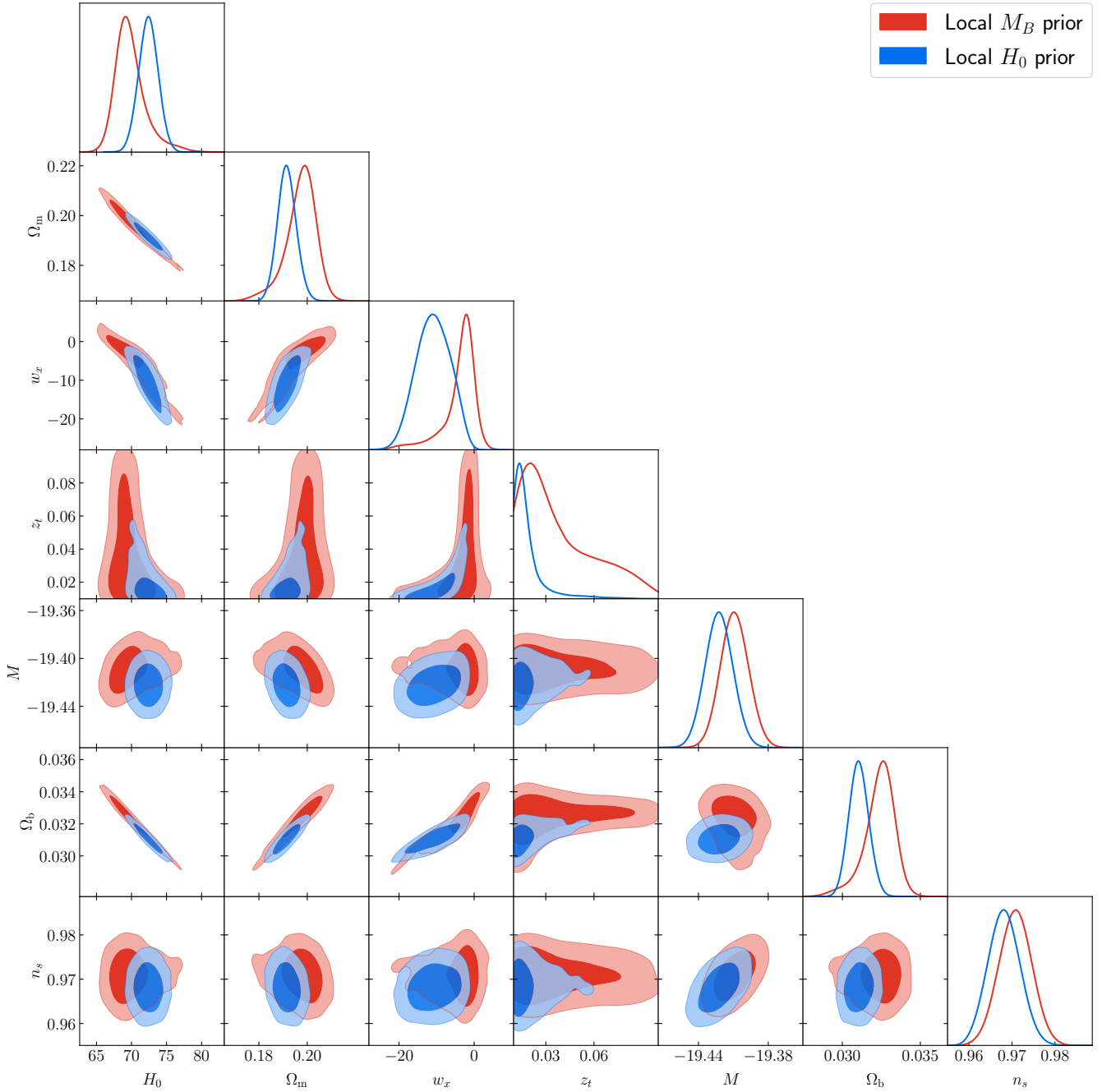


Figure 6. Marginalized constraints for hockey-stick dark energy ($hs\Lambda\text{CDM}$) from CMB, BAO, SNe and local observations. The two sets of contours show the analysis that adopts the prior on M_B of equation (9) and the one that adopts the prior on H_0 of equation (8). As explained in the text, the latter analysis both biases model selection and distorts the posterior.

References

- Aghanim N., et al., 2020, *Astron. Astrophys.*, 641, A6, [1807.06209].
- Alam S., et al., 2017, *Mon. Not. Roy. Astron. Soc.*, 470, 2617, [1607.03155].
- Aletras G., Kazantzidis L., Perivolaropoulos L., 2020, [2012.13932].
- Audren B., Lesgourgues J., Benabed K., Prunet S., 2013, *JCAP*, 1302, 001, [1210.7183].
- Benevento G., Hu W., Raveri M., 2020, *Phys. Rev. D*, 101, 103517, [2002.11707].
- Beutler F., et al., 2011, *Mon. Not. Roy. Astron. Soc.*, 416, 3017, [1106.3366].
- Blas D., Lesgourgues J., Tram T., 2011, *JCAP*, 1107, 034, [1104.2933].
- Brout D., Scolnic D., 2021, *Astrophys. J.*, 909, 26, [2004.10206].
- Brout D., et al., 2019, *Astrophys. J.*, 874, 150, [1811.02377].
- Camarena D., Marra V., 2020a, *Phys. Rev. Res.*, 2, 013028, [1906.11814].
- Camarena D., Marra V., 2020b, *Mon. Not. Roy. Astron. Soc.*, 495, 2630, [1910.14125].

- Chen L., Huang Q.-G., Wang K., 2019, *JCAP*, 02, 028, [1808.05724].
- Dhawan S., Brout D., Scolnic D., Goobar A., Riess A., Miranda V., 2020, *Astrophys. J.*, 894, 54, [2001.09260].
- Di Valentino E., et al., 2021, [2103.01183].
- Efstathiou G., 2021, [2103.08723].
- Foreman-Mackey D., Hogg D. W., Lang D., Goodman J., 2013, *Publ. Astron. Soc. Pac.*, 125, 306, [1202.3665].
- Goliath M., Amanullah R., Astier P., Goobar A., Pain R., 2001, *Astron. Astrophys.*, 380, 6, [astro-ph/0104009].
- Guy J., et al., 2007, *Astron. Astrophys.*, 466, 11, [astro-ph/0701828].
- Huang Z., 2020, *Astrophys. J. Lett.*, 892, L28, [2001.06926].
- Kang Y., Lee Y.-W., Kim Y.-L., Chung C., Ree C. H., 2020, *Astrophys. J.*, 889, 8, [1912.04903].
- Keeley R. E., Joudaki S., Kaplinghat M., Kirkby D., 2019, *JCAP*, 12, 035, [1905.10198].
- Kelly P. L., Hicken M., Burke D. L., Mandel K. S., Kirshner R. P., 2010, *ApJ*, 715, 743, [0912.0929].
- Kim Y.-L., Kang Y., Lee Y.-W., 2019, *J. Korean Astron. Soc.*, 52, 181, [1908.10375].
- Knox L., Millea M., 2020, *Phys. Rev. D*, 101, 043533, [1908.03663].
- Koo H., Shafieloo A., Keeley R. E., L’Huillier B., 2020, *Astrophys. J.*, 899, 9, [2001.10887].
- Lampeitl H., et al., 2010, *ApJ*, 722, 566, [1005.4687].
- Lemos P., Lee E., Efstathiou G., Gratton S., 2019, *Mon. Not. Roy. Astron. Soc.*, 483, 4803, [1806.06781].
- Lewis A., 2019, [1910.13970].
- Mortonson M. J., Hu W., Huterer D., 2009, *Phys. Rev. D*, 80, 067301, [0908.1408].
- Riess A. G., et al., 2016, *Astrophys. J.*, 826, 56, [1604.01424].
- Riess A. G., Casertano S., Yuan W., Bowers J. B., Macri L., Zinn J. C., Scolnic D., 2021, *Astrophys. J. Lett.*, 908, L6, [2012.08534].
- Rose B. M., et al., 2020, *Astrophys. J. Lett.*, 896, L4, [2002.12382].
- Ross A. J., Samushia L., Howlett C., Percival W. J., Burden A., Manera M., 2015, *Mon. Not. Roy. Astron. Soc.*, 449, 835, [1409.3242].
- Sapone D., Nesseris S., Bengaly C. A. P., 2020, [2006.05461].
- Scolnic D., et al., 2015, *Astrophys. J.*, 815, 117, [1508.05361].
- Scolnic D. M., et al., 2018, *Astrophys. J.*, 859, 101, [1710.00845].
- Sullivan M., et al., 2010, *MNRAS*, 406, 782, [1003.5119].

This paper has been typeset from a $\text{\TeX}/\text{\LaTeX}$ file prepared by the author.